

$NaBH_4$ induces strong ferromagnetism of $Bi_2Fe_4O_9$ at room temperature

Chong Wang(王冲), Guorong Liu(刘国荣), Xiaofeng Sun(孙小峰), Jinyuan Ma(马金元), Tao Xian(县涛), and Hua Yang(杨华)

Citation: Chin. Phys. B, 2025, 34 (**12**): 127503. DOI: 10.1088/1674-1056/ade855
http://cpb.iphy.ac.cn; http://iopscience.iop.org/cpb

What follows is a list of articles you may be interested in

Tunable anomalous Hall effect and anisotropic magnetism in In-doped $TbMn_6Sn_6$ kagome magnets

Detong Wu(吴德桐), Jianwei Qin(秦建伟), and Bing Shen(沈冰)
Chin. Phys. B, 2025, 34 (**10**): 107511. DOI: 10.1088/1674-1056/adde37

Thickness-dependent magnetic property of FeNi thin film grown on flexible graphene substrate

Suixin Zhan(詹遂鑫), Shaokang Yuan(袁少康), Yuming Bai(白宇明), Fu Liu(刘福), Bohan Zhang(张博涵), Weijia Han(韩卫家), Tao Wang(王韬), Shengxiang Wang(汪胜祥), and Cai Zhou(周偲)
Chin. Phys. B, 2025, 34 (**2**): 027503. DOI: 10.1088/1674-1056/ad92fd

Magnetic domain structures in ultrathin $Bi_2Te_3/CrTe_2$ heterostructures

Tirui Xia(夏体瑞), Xiaotian Yang(杨笑天), Yifan Zhang(张逸凡), Xinqi Liu(刘馨琪), Xinyu Cai(蔡新雨), Chang Liu(刘畅), Qi Yao(姚岐), Xufeng Kou(寇煦丰), and Wenbo Wang(王文波)
Chin. Phys. B, 2024, 33 (**8**): 087504. DOI: 10.1088/1674-1056/ad4a3a

Critical behavior of quasi-two-dimensional ferromagnet $Cr_{1.04}Te_2$

Wei Niu(钮伟), Qin-Xin Song(宋沁心), Shi-Qi Chang(常世琦), Min Wang(王敏), Kui Yuan(袁奎), Jia-Cheng Gao(高嘉程), Shuo Wang(王硕), Zhen-Dong Wang(王振东), Kai-Fei Liu(刘凯斐), Ping Liu(刘萍), Yong-Bing Xu(徐永兵), Xiao-Qian Zhang(张晓倩), and Yong Pu(普勇)
Chin. Phys. B, 2024, 33 (**7**): 077506. DOI: 10.1088/1674-1056/ad4cd8

Theoretical characterization of the temperature-dependent saturation magnetization of magnetic metallic materials

Jin-Long Wu(吴金龙), Pan Dong(董攀), Yi He(贺屹), Yan-Li Ma(马艳丽), Zi-Yuan Li(李梓源), Qin-Yuan Yao(姚沁远), Jun Qiu(邱俊), Jian-Zuo Ma(麻建坐), and Wei-Guo Li(李卫国)
Chin. Phys. B, 2024, 33 (**7**): 077502. DOI: 10.1088/1674-1056/ad39d1

$NaBH_4$ induces strong ferromagnetism of $Bi_2Fe_4O_9$ at room temperature

Chong Wang(王冲)[1], Guorong Liu(刘国荣)[1,†], Xiaofeng Sun(孙小峰)[2], Jinyuan Ma(马金元)[2], Tao Xian(县涛)[3], and Hua Yang(杨华)[1,2]

[1] *School of Science, Lanzhou University of Technology, Lanzhou* 730050, *China*
[2] *State Key Laboratory of Advanced Processing and Recycling of Non-ferrous Metals, Lanzhou University of Technology, Lanzhou* 730050, *China*
[3] *College of Physics and Electronic Information Engineering, Qinghai Normal University, Xining* 810008, *China*

(Received 23 April 2025; revised manuscript received 25 June 2025; accepted manuscript online 26 June 2025)

$Bi_2Fe_4O_9$ nanosheets were prepared using a hydrothermal method, followed by the introduction of $NaBH_4$ and high-temperature calcination, which successfully induced strong ferromagnetism in the material at room temperature (M_S = 10.22 emu/g and M_r = 2.93 emu/g). This work demonstrates for the first time that $Bi_2Fe_4O_9$ can exhibit such strong ferromagnetism at room temperature, with potential for further enhancements. Meanwhile, the ferroelectric properties of the samples were investigated. X-ray diffraction confirmed that the samples were single-phase with no detectable impurities. Based on a series of characterization analyses, it is inferred that Bi vacancies contribute to the observed strong magnetism.

Keywords: $Bi_2Fe_4O_9$, strong ferromagnetism, room temperature, $NaBH_4$

PACS: 75.75.Cd, 75.85.+t, 77.55.Nv

DOI: 10.1088/1674-1056/ade855 **CSTR:** 32038.14.CPB.ade855

1. Introduction

Since the magneto-electric coupling effect was predicted by Curie in 1894,[1] materials possessing both ferromagnetic and ferroelectric properties, i.e., multiferroic materials, at room temperature have been actively pursued.[2] Due to their ability to manipulate both electrical and magnetic properties, such materials hold great potential for applications in spintronic devices, sensors, and data storage systems.[3–9] In the 1960s, a weak magnetoelectric coupling phenomenon was discovered in Cr_2O_3.[10] Over the subsequent decades, the search for multiferroic materials faced numerous challenges and achieved limited progress. From the perspective of symmetry, ferromagnetism arises from the breaking of time-reversal symmetry, whereas ferroelectricity results from the breaking of spatial inversion symmetry. From the viewpoint of solid-state band theory, ferromagnetic order requires a small band gap, whereas ferroelectric order favors a large band gap. Owing to these distinct and often conflicting mechanisms, for a long time, not only were materials exhibiting both ferromagnetism and ferroelectricity not found, but even materials combining antiferromagnetism and ferroelectricity were extremely rare. Until 2003, the discovery of epitaxial $BiFeO_3$ multiferroic thin-film heterostructures heralded a renaissance in this field.[11]

As a material exhibiting both antiferromagnetism and ferroelectricity at room temperature, $BiFeO_3$ has recently attracted considerable attention.[12–16] $Bi_2Fe_4O_9$, a byproduct in the production of $BiFeO_3$, also possesses multiferroic properties and a rich array of physical characteristics near room temperature. However, it has not received substantial attention and remains relatively unexplored.

$Bi_2Fe_4O_9$ has long been regarded as antiferromagnetic at low temperatures (264 ± 3 K) and paramagnetic at room temperature.[17] Qiu *et al.* enhanced its magnetic properties through Cr doping, with the optimal composition $Bi_2Fe_{3.68}Cr_{0.32}O_9$ achieving a remanent magnetization (M_r) of 0.025 emu/g.[18] Tian *et al.* studied the size-dependent magnetic properties of $Bi_2Fe_4O_9$ nanoparticles using an improved Pechini method, finding that 60 nm nanoparticles reached a saturation magnetization (M_S) of 0.58 emu/g.[19] They also enhanced magnetic properties via Ti doping, with $Bi_2Fe_{3.7}Ti_{0.3}O_9$ reaching M_r = 0.0188 emu/g.[20] Mohapatra *et al.* investigated Co doping, resulting in M_r increasing from 0.00078 emu/g for $Bi_2Fe_4O_9$ to 0.1401 emu/g for $Bi_2Fe_{3.92}Co_{0.08}O_9$, representing an enhancement of approximately 180 times.[21] Furthermore, other doping strategies and compositing have been attempted, leading to slight ferromagnetic enhancements at room temperature; however, achieving macroscopic magnetism without magnetic impurities remains challenging.[22–25]

Building on these studies, we report a novel approach to enhance the magnetic properties of $Bi_2Fe_4O_9$ by introducing $NaBH_4$ for high-temperature calcination, successfully inducing strong room-temperature ferromagnetism (M_S = 10.22 emu/g and M_r = 2.93 emu/g). A comparison with previous works is provided in Table S1. To the best of our knowl-

†Corresponding author. E-mail: liugr07@163.com

© 2025 Chinese Physical Society and IOP Publishing Ltd. All rights, including for text and data mining, AI training, and similar technologies, are reserved.

edge, this is the first report of $Bi_2Fe_4O_9$ exhibiting such strong ferromagnetism at room temperature, with potential for further enhancements. X-ray diffraction (XRD) confirmed that all samples are single-phase with no detectable impurities. Additionally, the ferroelectric properties of the samples were investigated. Through a series of techniques including ICP-OES, XPS, SEM, and Raman spectroscopy, we deduced that Bi vacancies contribute to the observed magnetism.

2. Experimental details

Step one Preparation of $Bi_2Fe_4O_9$ nanosheets.[26] 2.0613 g of $Bi(NO_3)_3{\cdot}5H_2O$ and 1.3515 g of $FeCl_3{\cdot}6H_2O$ were dissolved in 50 ml of ethylene glycol under magnetic stirring. Then, 200 ml of deionized (DI) water was added, and the pH was adjusted to 11 by dropwise addition of concentrated ammonia. The resulting brown precipitate was washed with DI water and subsequently added to 40 ml of 14 mol/L NaOH solution. After thorough stirring, the mixture was transferred to a 100 ml autoclave and sealed. Following a 72-hour hydrothermal treatment at 180 °C, the sample was ultrasonicated in 2 mol/L nitric acid for 30 min to remove impurities, then washed repeatedly with DI water and ethanol, and dried at 70 °C. The prepared $Bi_2Fe_4O_9$ nanosheets are referred to as BFO.

Step Two Modification of $Bi_2Fe_4O_9$. Firstly, 0.05 mol of BFO and $NaBH_4$ (1:1) were thoroughly ground in an agate mortar to form a homogeneous mixture, which was placed in a porcelain boat. The mixture was then calcined at 300 °C or 400 °C in a tube furnace under argon for 1 h. The resulting samples were washed with DI water and ethanol. Subsequently, the samples were repeatedly treated with excess nitric acid under ultrasonication at 60 °C to remove residual impurities, followed by washing again with DI water and ethanol and drying at 70 °C. The samples obtained at 300 °C and 400 °C are referred to as BFO-1NH-300 and BFO-1NH-400, respectively. The sample obtained at 400 °C with a BFO : $NaBH_4$ ratio of 0.05 mol : 0.075 mol (1 : 1.5) is referred to as BFO-1.5NH-400. In control experiments, the sample obtained without $NaBH_4$ at 400 °C is referred to as BFO-400.

3. Results and discussion

XRD data were recorded to characterize the crystal structure of the samples, as shown in Fig. S1. All diffraction peaks of the BFO nanosheets and calcined samples match PDF#25-0090. Rietveld refinement of XRD patterns for BFO and BFO-1.5NH-400 indicates that the diffraction peaks can be accurately refined to the orthorhombic $Bi_2Fe_4O_9$ mullite structure, with space group *Pbam*55 (Figs. 1(a) and 1(b)). No extraneous peaks were observed, confirming the purity of the samples. Notably, high-temperature calcination did not alter the crystal structure of the BFO nanosheets. After repeated washing with nitric acid under ultrasonication, the samples remained pure single-phase $Bi_2Fe_4O_9$. Quantitative elemental analysis using inductively coupled plasma atomic emission spectroscopy (ICP-OES) (Fig. 1(c)) shows Bi/Fe atomic ratios of 1.02:2 in BFO and 1.03:2 in BFO-400, which decrease to 0.79:1 in BFO-1.5NH-400, indicating that $NaBH_4$ treatment introduced approximately 20% Bi vacancies in the material.[27,28]

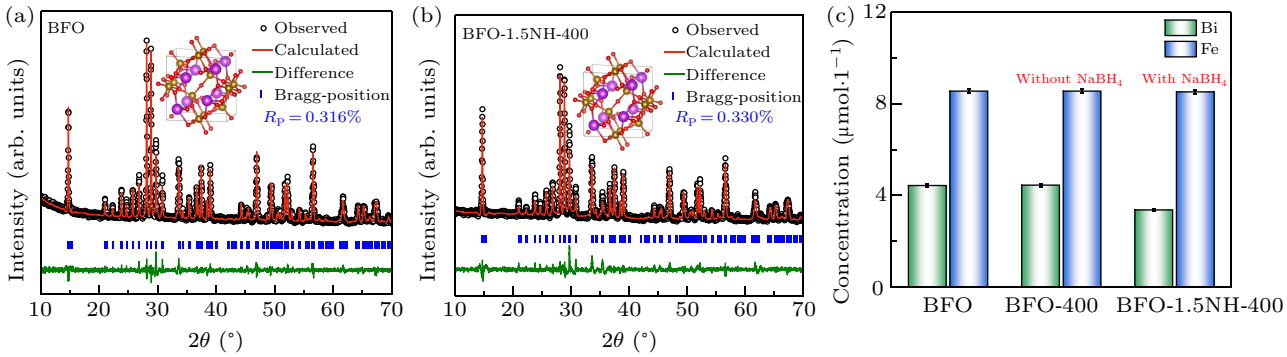


Fig. 1. (a) and (b) The Rietveld-refined XRD patterns of BFO and BFO-1.5NH-400, respectively; (c) ICP-OES analysis. The Bi and Fe contents are normalized.

Based on this, we conducted controlled experiments on BFO-1.5NH-400, recording XRD data before and after nitric acid treatment, as well as after calcination without the addition of $NaBH_4$ (Fig. S2). The results revealed that under identical experimental conditions, BFO-1.5NH-400*, which had not been washed with nitric acid after calcination, exhibited peaks corresponding to Bi (PDF#01-0699) at 27.23°, 38.03°, and 39.73°, as well as Bi_2O_3 (PDF#29-0236) at 31.88°, 32.79°, and 46.23°. In contrast, for BFO-400 without $NaBH_4$ under the same conditions, these heterogeneous peaks were absent, indicating that $NaBH_4$ treatment induces the formation of Bi and Bi_2O_3, rather than resulting from high-temperature calcination alone. Due to the tendency of Bi powder to oxidize in air forming Bi_2O_3, it is suggested that $NaBH_4$ induces Bi atom precipitation from BFO, generating Bi vacancies. Additionally, a comparison of the resistivity of BFO and BFO-1.5NH-

400 at room temperature (Fig. S3) revealed no evidence of a transition to an insulating phase, ruling out the incorporation of H ions into the lattice.[29,30] During calcination, the reaction between $Bi_2Fe_4O_9$ and $NaBH_4$ can be represented by[31,32]

$$2NaBH_4 \rightarrow 2NaH + B_2 + 3H_2, \quad (1)$$

$$Bi_2Fe_4O_9 + 3xH_2 \rightarrow Bi_{2-2x}Fe_4O_{9-3x} + 2xBi + 3xH_2O. \quad (2)$$

SEM observations of the microstructural morphologies of the samples are shown in Fig. S4. BFO exhibited a square flake shape. After calcination, the surface of BFO-1.5NH-400 displayed numerous porous bubbles, while its overall morphology remained largely unchanged. EDS elemental spectra were obtained for semi-quantitative analysis (Fig. S5), revealing significant Bi deficiency in the calcined samples.

X-ray photoelectron spectroscopy (XPS) was employed to characterize surface valence states before and after the reaction (Fig. 2). In the Fe 2p spectrum (Fig. 2(a)), the Fe $2p_{3/2}$ peak at 710.8 eV was deconvoluted into two peaks at 711.3 eV and 710.1 eV, corresponding to Fe^{3+} and Fe^{2+}, respectively, indicating the coexistence of Fe^{3+} and Fe^{2+} in $Bi_2Fe_4O_9$ nanosheets. The presence of Fe^{2+} arises from unavoidable oxygen deficiency during sample preparation.[33] The content of Fe^{2+} is minimal, with no significant change before and after reaction. The O 1s peaks were deconvoluted into three components at 529.9 eV, 531.6 eV, and 533 eV, corresponding to lattice oxygen O_L, oxygen vacancies O_V, and adsorbed water/oxygen O_{H_2O}, respectively (Fig. 2(b)). The content of O_V increases after calcination, consistent with Bi precipitation observed in XRD and electrical neutrality considerations. This trend aligns with the reactions described in Eqs. (1) and (2). In Fig. 2(c), Bi $4f_{7/2}$ and Bi $4f_{5/2}$ peaks shift slightly to higher binding energies after high-temperature calcination, reflecting reduced outer electron density and weakened shielding due to Bi vacancy formation. Semi-quantitative XPS analysis of different samples (Table S2) shows a gradual decrease in Bi content.

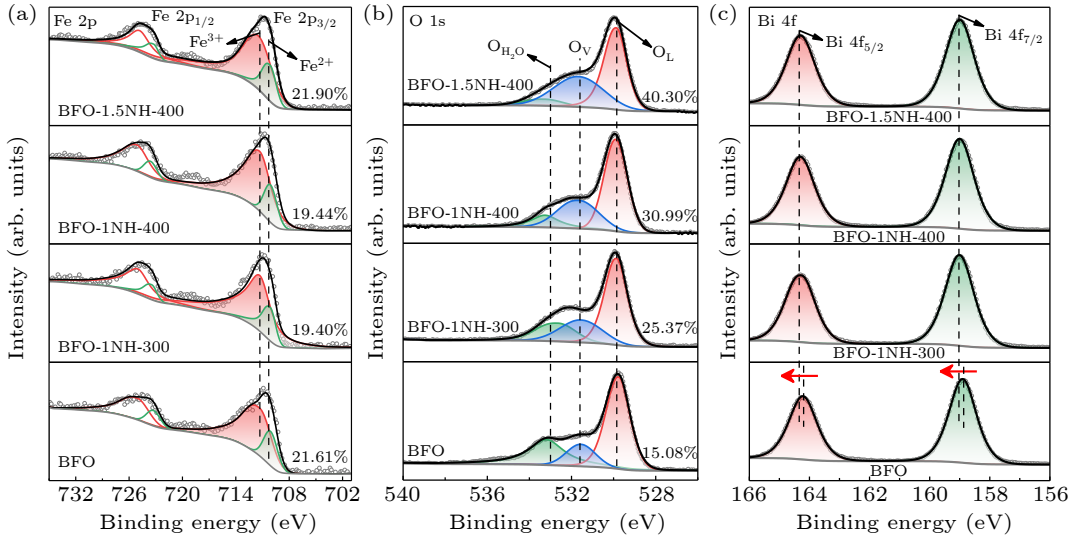


Fig. 2. High-resolution XPS spectra of BFO, BFO-1NH-300, BFO-1NH-400, and BFO-1.5NH-400. (a) Fe 2p, (b) O 1s, and (c) Bi 4f.

The ferromagnetic properties of the different samples were measured at room temperature using VSM over a magnetic field range of ±2 T (Fig. 3(a)). The BFO samples exhibited paramagnetic behavior, consistent with previous reports. In contrast, the calcined samples displayed clear ferromagnetic hysteresis loops. Ferromagnetic properties progressively improved with increasing calcination temperature and $NaBH_4$ content, with BFO-1.5NH-400 reaching a maximum saturation magnetization of $M_s = 10.22$ emu/g, near saturation at 0.25 T. The remanent magnetization was $M_r = 2.93$ emu/g, and the coercivity was $H_c = 221.5$ Oe (Fig. 3(b)). Ferromagnetic properties are expected to increase further with higher calcination temperature and $NaBH_4$ content. To the best of our knowledge, such strong ferromagnetism in this material has not been previously reported. Macroscopic magnetic behaviors at room temperature are compared in supplementary information 2.

To further investigate magnetic properties, the temperature dependence of zero-field-cooled (ZFC) and field-cooled (FC) magnetization was recorded under an applied magnetic field of 0.05 T (Figs. 3(c) and 3(d)). As the temperature decreased, a peak was observed in BFO around 250 K, corresponding to the Néel temperature (T_N) for the paramagnetic-to-antiferromagnetic transition. Below T_N, the ZFC and FC curves continued to decline and then increased in the low-temperature region, consistent with previous reports.[24] For BFO-1.5NH-400, a continuous splitting of the ZFC and FC curves was observed, indicative of typical ferromagnetic behavior.

In addition, the ferroelectric polarization–electric field (P–E) hysteresis loop of BFO-1.5NH-400 was measured at room temperature at 1 kHz, as shown in Fig. S6. Due to the

leakage current caused by defects, the hysteresis loop exhibited an inclined elliptical shape, consistent with previous reports on the ferroelectric properties of $Bi_2Fe_4O_9$.[19,20,34,35] To further investigate the ferroelectric behavior, current–voltage (I–V) curves were measured at room temperature (Fig. S7). Generally, the I–V curve reflects the superposition of displacement current and leakage current.[36] Figure S7 shows a thick rectangular shape, further confirming the presence of significant leakage current, a phenomenon attributable to the intrinsic properties of bismuth ferrite and the effect of powdered material. Due to the combination of large leakage current and relatively small displacement current, only minor switching peaks near 2772 V and −2838 V were observed, suggesting weak ferroelectricity in the sample.

Raman scattering spectra of BFO and BFO-1.5NH-400 were recorded at room temperature and deconvoluted for analysis. According to group theoretical irreducible representations, orthorhombic $Bi_2Fe_4O_9$ possesses 42 Raman-active modes ($12A_g + 12B_{1g} + 9B_{2g} + 9B_{3g}$).[37] Due to the low polarizability of certain modes, fewer characteristic peaks were observed, consistent with previous reports.[38] As shown in Fig. 4(b), the Raman spectra of both samples exhibit typical $Bi_2Fe_4O_9$ peaks. In BFO, peaks at 59 cm^{-1}, 79 cm^{-1}, and 109 cm^{-1} correspond to the $B_{2g}(1)$, $A_g(1)$, and $B_{1g}(2)$ modes, respectively, attributed to vibrational modes of Bi atoms in the lattice.[37] The peak at 197 cm^{-1} is ascribed to Fe_1 tetrahedron vibrations, while peaks at 275 cm^{-1}, 317 cm^{-1}, 363 cm^{-1}, 415 cm^{-1}, and 537 cm^{-1} correspond to Fe_2 octahedron vibrations.[37–39] Table S3 summarizes the specific Raman modes corresponding to these peaks.

For BFO-1.5NH-400, the $B_g(1)$ mode at 59 cm^{-1} observed in BFO was absent. Additionally, the $B_{1g}(2)$ peak at 107 cm^{-1} shifted, broadened, and decreased in intensity, attributed to increased lattice disorder caused by Bi vacancies.[40] Furthermore, all characteristic peaks exhibited a redshift, indicating overall lattice distortion.[41] However, the peak at 207 cm^{-1} showed an anomalous blueshift, where the Raman mode corresponds to Fe_1 atomic motion within the x–y plane.

For the $Bi_2Fe_4O_9$ structure in Fig. 4(a), the Fe_1 and Fe_2 atoms are antiferromagnetically and ferromagnetically coupled, respectively, with five major magnetic superexchange interactions between them, denoted J_1 to J_5.[42] The projections of J_3 to J_5 along the c-axis form a distorted pentagonal Cairo lattice (Fig. 4(c)) that exhibits significant spin frustration.[43] This intrinsic spin frustration prevents macroscopic ferromagnetism in $Bi_2Fe_4O_9$ at room temperature. In contrast, J_4, dominated by Fe_1, exhibits the strongest superexchange interaction in the lattice due to the Fe–O–Fe bond angle of 180°.[44] Bi vacancies affect the Fe atoms. Based on the large blueshift of Fe_1 atoms in the Raman spectra, this anomaly may disrupt the Cairo pentagonal spin arrangement of Fe_1 atoms, leading to the macroscopic magnetism observed in BFO-1.5NH-400.

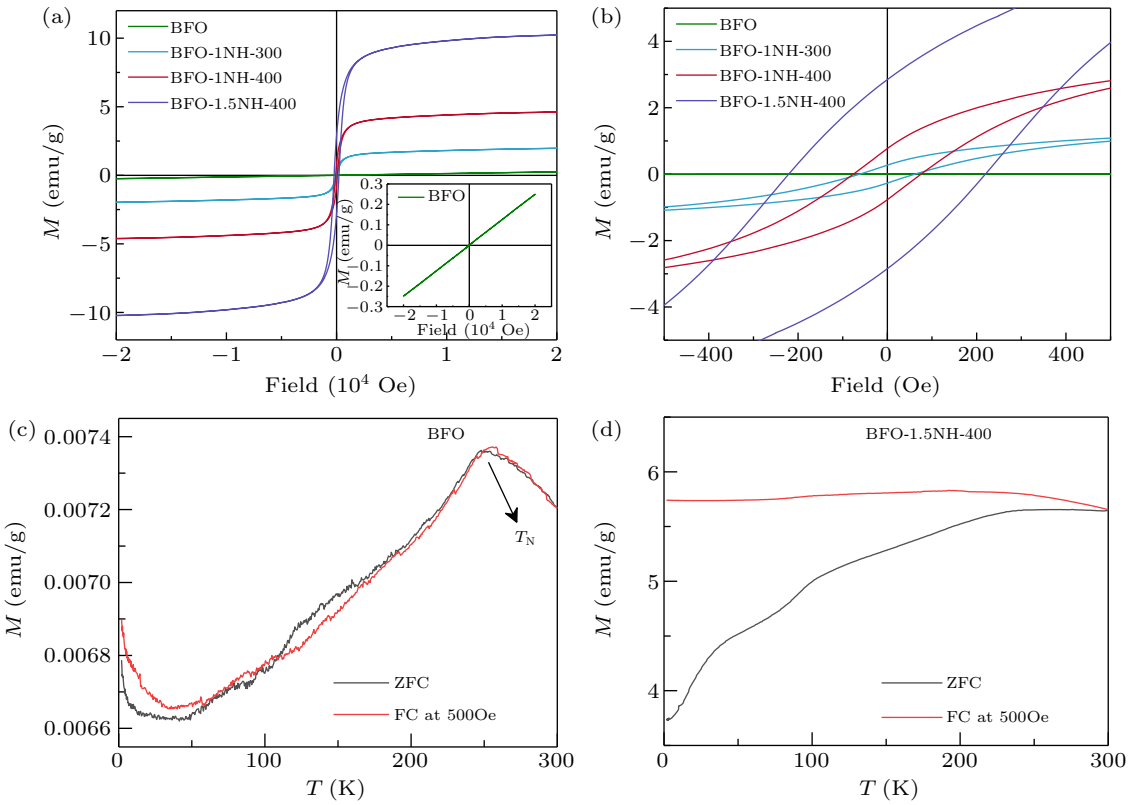


Fig. 3. (a) Magnetization (M–H) hysteresis loops of BFO, BFO-1NH-300, BFO-1NH-400, and BFO-1.5NH-400, with the inset showing an enlarged M–H loop of BFO; (b) M–H curves near $H = 0$. (c) and (d) The zero-field-cooled (ZFC) and field-cooled (FC) magnetization curves of BFO and BFO-1.5NH-400, respectively.

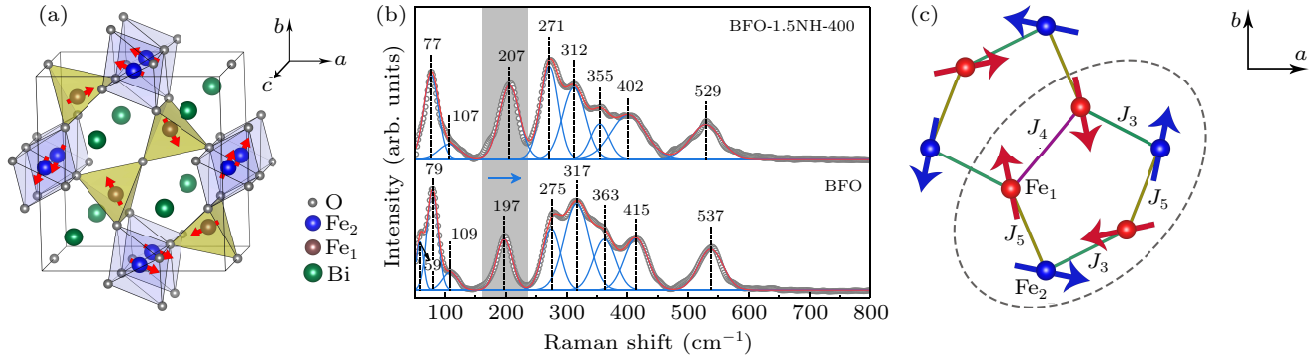


Fig. 4. (a) Crystal structure of $Bi_2Fe_4O_9$, with arrows indicating spin orientations. (b) Raman spectra of BFO and BFO-1.5NH-400. (c) Schematic of spin frustration in the Cairo pentagonal lattice.

Furthermore, the ferromagnetism induced by Bi vacancies in $Bi_2Fe_4O_9$ has been supported by density functional theory calculations proposed by Kajal *et al.*[45] Theoretical results showed that Bi vacancies induce spin polarization in Fe d orbitals and O p orbitals near the Fermi level, which are the primary origin of the net magnetic moment in $Bi_2Fe_4O_9$.

In summary, this paper reports a novel approach to induce strong ferromagnetism in $Bi_2Fe_4O_9$ at room temperature via $NaBH_4$ treatment. Characterization data confirm that the material remains a pure single-phase $Bi_2Fe_4O_9$ with significant Bi vacancies. A mechanism for the origin of the magnetism is also proposed. This strong ferromagnetism in $Bi_2Fe_4O_9$ has not been previously reported. We anticipate that this discovery will enhance understanding of the magnetic properties of this material and provide new insights into the study of multiferroics.

Acknowledgments

This work was supported by the Natural Science Foundation of Gansu Province of China (Grant No. 24JRRA171), the Postgraduate "Innovative Star" Project of Gansu Provincial Department of Education (Grant No. 2025CXZX-587), and the National Natural Science Foundation of China (Grant No. 52162040).

References

[1] Curie P 1894 *J. Phys. Theor. Appl.* **3** 393
[2] Schmid H 1994 *Ferroelectrics* **162** 317
[3] Catalan G and Scott J F 2009 *Adv. Mater.* **21** 2463
[4] Safi R and Shokrollahi H 2012 *Prog. Solid State Chem.* **40** 6
[5] Allibe J, Fusil S, Bouzehouane K, Daumont C, Sando D, Jacquet E, Deranlot C, Bibes M and Barthelemy A 2012 *Nano Lett.* **12** 1141
[6] Poghossian A S, Abovian H V, Avakian P B, Mkrtchian S H and Haroutunian V M 1991 *Sens. Actuators B* **4** 545
[7] Wang T, Xu Y, Liu Y, Dai X, Yan P, Wang J, Wang S, Deng Y, He K, Li C, Wang Z, Zou W, Wen R, Hao Y and He L 2024 *Chin. Phys. Lett.* **41** 107502
[8] Zha H, Li W, Zhang G, Liu W, Deng L, Jiang Q, Ye M, Wu H, Chang H and Qiao S 2023 *Chin. Phys. Lett.* **40** 087501
[9] Peng X, Si M and Gao D 2024 *Chin. Phys. B* **33** 017503
[10] Dzyaloshinskii I E 1960 *Sov. Phys. JETP* **10** 628
[11] Wang J, Neaton J B, Zheng H, Nagarajan V, Ogale S B, Liu B, Viehland D, Vaithyanathan V, Schlom D G, Waghmare U V, Spaldin N A, Rabe K M, Wuttig M and Ramesh R 2003 *Science* **299** 1719
[12] Young S M, Zheng F and Rappe A M 2012 *Phys. Rev. Lett.* **109** 236601
[13] Seidel J, Fu D, Yang S Y, Alarcó-Lladó E, Wu J, Ramesh R and Ager III J W 2011 *Phys. Rev. Lett.* **107** 126805
[14] Zeches R J, Rossell M D, Zhang J X, Hatt A J, He Q, Yang C H, Kumar A, Wang C H, Melville A, Adamo C, Sheng G, Chu Y H, Ihlefeld J F, Erni R, Ederer C, Gopalan V, Chen L Q, Schlom D G, Spaldin N A, Martin L W and Ramesh R 2009 *Science* **326** 977
[15] Bhatnagar A, Roy C A, Heon K Y, Hesse D and Alexe M 2013 *Nat. Commun.* **4** 2835
[16] Choi T, Lee S, Choi Y J, Kiryukhin V and Cheong S W 2009 *Science* **324** 63
[17] Shamir N, Gurewitz E and Shaked H 1978 *Acta Crystallogr. A* **34** 662
[18] Qiu Y, Zou Z J, Sang R R, Wang H, Xue D, Tian Z M, Gong G S and Yuan S L 2015 *J. Mater. Sci.: Mater. Electron.* **26** 1732
[19] Tian Z M, Yuan S L, Wang X L, Zheng X F, Yin S Y, Wang C H and Liu L 2009 *J. Appl. Phys.* **106** 103912
[20] Tian Z M, Qiu Y, Yuan S L, Wu M S, Huo S X and Duan H N 2010 *J. Appl. Phys.* **108** 064110
[21] Mohapatra S R, Sahu B, Chandrasekhar M, Kumar P, Kaushik S D, Rath S and Singh A K 2016 *Ceram. Int.* **42** 12352
[22] Pooladi M, Sharifi I and Behzadipour M 2020 *Ceram. Int.* **46** 18453
[23] Raghavan C M, Kim J W, Choi J Y, Kim J W and Kim S S 2014 *Ceram. Int.* **40** 14165
[24] Rao S K, Abhinav E M, Jaison D, Sundararaj A, Santhiya M, Althaf R and Gopalakrishnan C 2020 *Vacuum* **172** 109109
[25] Yuan X, Shi L, Zhao J, Zhou S and Guo J 2018 *Scr. Mater.* **146** 55
[26] Su C, Li R, Li C and Wang W 2022 *Appl. Catal. B* **310** 121330
[27] Liu B, Wang X, Zhang Y, Wan K, Xu L, Ma S, Zhao R, Wang S and Huang W 2024 *Adv. Energy Mater.* 2403835
[28] Lu Y, Yang Y, Fan X, Li Y, Zhou D, Cai B, Wang L, Fan K and Zhang K 2022 *Adv. Mater.* **34** 2108178
[29] Yuan Y, Kotiuga M, Park T J, Patel R K, Ni Y, Saha A, Zhou H, Sadowski J T, Mahboob A A, Yu H, Du k, Zhu M, Deng S, Bisht R S, Lyu X, Wu C T M, Ye P D, Sengupta A, Cheong S W, Xu X, Rabe K M and Ramanathan S 2024 *Nat. Commun.* **15** 4717
[30] Gamage S, Manna S, Zajac M, Hancock S, Wang Q, Singh S, Ghafariasl M, Yao K, Tiwald T E, Park T J, Landau D P, Wen H, Sankaranarayanan S K R S, Darancet P, Ramanathan S and Abate Y 2024 *ACS Nano* **18** 2105
[31] Martelli P, Caputo R, Remhof A, Mauron P, Borgschulte A and Zuttel A 2010 *J. Phys. Chem. C* **114** 7173
[32] Wang Y, Sun X, Ma J, Yi Z, Wang S, Liu G and Yang H 2024 *Sep. Purif. Technol.* **337** 126392
[33] Du Y, Lu T, Li X, Liu Y, Sun W, Zhang S and Cheng Z 2022 *Nano Energy* **104** 107919
[34] Dutta D P, Sudakar C, Mocherla P S, Mandal B P, Jayakumar O D and Tyagi A K 2012 *Mater. Chem. Phys.* **135** 998
[35] Ma F and Zhao H 2019 *Russ. J. Phys. Chem. A* **93** 2079
[36] Meyer R, Waser R, Prume K, Schmitz T and Tiedke S 2005 *Appl. Phys. Lett.* **86** 142907
[37] Iliev M N, Litvinchuk A P, Hadjiev V G, Gospodinov M M, Skumryev V and Ressouche E 2010 *Phys. Rev. B* **81** 024302

[38] Hua H, Feng F, Du M, Ma Y, Pu Y, Zhang J and Li X A 2021 *Appl. Surf. Sci.* **541** 148428
[39] Su C, Li C, Li R and Wang W 2023 *Chem. Eng. J.* **452** 139300
[40] Kitajima M 1997 *Crit. Rev. Solid State Mater. Sci.* **22** 275
[41] Liu H, Li L, Guo C, Ning J, Zhong Y and Hu Y 2020 *Chem. Eng. J.* **385** 123929
[42] Ressouche E, Simonet V, Canals B, Gospodinov M and Skumryev V 2009 *Phys. Rev. Lett.* **103** 267204
[43] Beauvois K, Simonet V, Petit S, Robert J, Bourdarot F, Gospodinov M, Mukhhin A A, Ballou R and Skumryev V 2020 *Phys. Rev. Lett.* **124** 127202
[44] Pchelkina Z V and Streltsov S V 2013 *Phys. Rev. B* **88** 054424
[45] Jindal K, Ameer S, Tomar M, Jha P K and Gupta V 2021 *Mater. Today Proc.* **47** 1637